Landmark-Based Elastic Registration Using Approximating Thin-Plate Splines

K. Rohr*, H. S. Stiehl, R. Sprengel, T. M. Buzug, J. Weese, and M. H. Kuhn

***Abstract*—We consider elastic image registration based on a set of corresponding anatomical point landmarks and approximating thin-plate splines. This approach is an extension of the original interpolating thin-plate spline approach and allows to take into account landmark localization errors. The extension is important for clinical applications since landmark extraction is always prone to error. Our approach is based on a minimizing functional and can cope with isotropic as well as anisotropic landmark errors. In particular, in the latter case it is possible to include different types of landmarks, e.g., unique point landmarks as well as arbitrary edge points. Also, the scheme is general with respect to the image dimension and the order of smoothness of the underlying functional. Optimal affine transformations as well as interpolating thin-plate splines are special cases of this scheme. To localize landmarks we use a semi-automatic approach which is based on three-dimensional (3-D) differential operators. Experimental results are presented for two–dimensional as well as 3-D tomographic images of the human brain.**

***Index Terms*—Anatomical landmarks, image matching, segmentation, splines.**

I. Introduction and Motivation

In neurosurgery and radiotherapy planning it is important to either register images from different modalities, e.g., magnetic resonance (MR) and X-ray computed tomography (CT) images, or to match images to atlas representations. If only *rigid* transformations are applied, then the accuracy of the resulting match often is not satisfactory with respect to clinical requirements. In general, *nonrigid* transformations are required to cope with the variations between the datasets. A special class of general nonrigid transformations are *elastic* transformations which allow for local adaptation and are constrained to some kind of continuity or smoothness.

This contribution is concerned with elastic registration of medical image data based on a set of corresponding anatomical landmarks. Such a landmark-based approach comprises three steps: 1) extraction of landmarks in the different datasets; 2) establishing the correspondence between the landmarks; and 3) computing the transformation between the datasets using the information from 1) and 2). Among the different types of landmarks (points, lines, surfaces, and volumes) we here consider point landmarks.

Previous work on point-based elastic registration has concentrated on a) selecting the corresponding landmarks manually and on b) using an interpolating transformation model (e.g., [2], [7], and [11]). The basic approach draws upon thin-plate splines or other splines and is computationally efficient. However, an interpolation scheme forces the corresponding landmarks to exactly match each other. The underlying assumption is that the landmark positions are known exactly. In real applications, however, landmark extraction is always prone to error.

Therefore, to take into account these landmark localization errors, we propose an approximation scheme, where the corresponding thin-plate splines result from a minimizing functional [13]–[15]. With this approach it is possible to individually weight the landmarks according to their localization uncertainty and thus to control the influence of the landmarks on the registration result. The localization uncertainties can be characterized either by scalar weights or, more generally, by weight matrices representing landmark error ellipsoids. In the latter case, anisotropic errors can be taken into account. This extension allows to include not only "normal" point landmarks, which have a unique position in all directions. In addition, we can include "quasi-landmarks" which are not uniquely definable in all directions, e.g., arbitrary edge points. Such landmarks are used, for example, in the reference system of Talairach [16] to define the three-dimensional (3-D) bounding box of the human brain. The incorporation of such landmarks is important since normal point landmarks are hard to define, for example, at the outer parts of the human head. To provide the elastic registration scheme with landmarks we use a semi-automatic procedure which is based on 3-D differential operators. Algorithms for landmark localization are important for clinical applications since manual selection of landmarks is time-consuming and often lacks accuracy.

Approximation schemes for point-based elastic registration have so far not been a focus of research. Bookstein [3] uses a linear regression model and a technique called "curve décolletage" to relax the interpolation condition. This approach has not been related to a minimizing functional with respect to the searched transformation and has only been applied to two–dimensional (2-D) synthetic data [simulated positron emission tomography (PET) images]. Recently, Christensen *et al.* [5] introduced a hierarchical approach to image registration combining a landmark-based scheme with an intensity-based scheme using

Manuscript received December 21, 1997; revised February 5, 2001. This work was supported by Philips Research Laboratories, Hamburg, Germany, under Project IMAGINE (IMage- and Atlas-Guided Interventions in NEurosurgery). The Associate Editor responsible for coordinating the review of this paper and recommending its publication was D. Hawkes. *Asterisk indicates corresponding author.*

*K. Rohr is with the School of Information Technology, International University in Germany, 76646 Bruchsal, Germany (e-mail: rohr@i-u.de).

H. S. Stiehl is with the Department of Computer Science, University of Hamburg, 22527 Hamburg, Germany.

R. Sprengel is with debis Systemhaus GEI, 22339 Hamburg, Germany.

T. M. Buzug is with the University of Applied Sciences Remagen, 53424 Remagen, Germany.

J. Weese and M. H. Kuhn are with Philips Research Laboratories, 22335 Hamburg, Germany.

Publisher Item Identifier S 0278-0062(01)03555-8.

a fluid model. The landmark scheme is based on the linear elasticity operator and the applied splines are different from thin-plate splines. Another difference to our approach is that the non-affine part of the transformation is separated from the affine part in their functional. While the stated functional allows to treat anisotropic errors in one of the two images to be registered, in their application only equal isotropic errors have been included. Finally, we mention the intensity-based approach of Gee *et al.* [8], which allows to integrate isotropic landmark errors. This approach, however, is not based on an analytic solution of the underlying functional but solves it numerically by applying the finite-element method (FEM), which is computationally much more expensive.

The remainder of this contribution is organized as follows. First, we briefly review the original thin-plate spline interpolation scheme and then we describe an extension to an approximation scheme. After that, we introduce a semi-automatic approach to the localization of 3-D anatomical point landmarks. Experimental results are presented for 2-D as well as 3-D tomographic images of the human brain.

II. Approximating Thin-Plate Splines for Elastic Image Registration

In this section, we first describe the interpolating thin-plate spline approach in the general context of registering d-dimensional image data. Then, we introduce an extension of this approach to an approximation scheme, which is based on the mathematical work of Duchon [6] and Wahba [20]. With this scheme it is possible to incorporate isotropic as well as anisotropic landmark errors.

A. Interpolating Thin-Plate Splines

Thin-plate spline interpolation can be stated as a multivariate interpolation problem: Given a number n of corresponding point landmarks $\mathbf{p}_i$ and $\mathbf{q}_i, i = 1, \ldots, n$ in two images of dimension d, find a continuous transformation $\mathbf{u} : \mathbb{R}^d \rightarrow \mathbb{R}^d$ within a suitable Hilbert space $\mathcal{H}$ of admissible functions, which 1) minimizes a given functional $J : \mathcal{H} \rightarrow \mathbb{R}$ and 2) fulfills the interpolation conditions

$$\mathbf{q}_i = \mathbf{u}(\mathbf{p}_i), \quad i = 1, \ldots, n. \tag{1}$$

Bookstein [2] proposed the use of thin-plate spline interpolation for point-based registration and applied this scheme to 2-D images. Application to 3-D image data has been reported in Evans *et al.* [7], for example. With this approach the minimizing functional represents the bending energy of a thin plate separately for each component $u_k, k = 1, \ldots, d$ of the transformation $\mathbf{u}$. Thus, the functional $J(\mathbf{u})$ can be separated into a sum of similar functionals each of which only depends on one component u_k of $\mathbf{u}$. Therefore the problem of finding $\mathbf{u}$ can be decomposed into d problems.

In the case of d-dimensional images and for an arbitrary order m of derivatives in the functional we have

$$J_m^d(\mathbf{u}) = \sum_{k=1}^{d} J_m^d(u_k) \tag{2}$$

where the single functionals read as

$$J_m^d(u) = \sum_{\alpha_1 + \cdots + \alpha_d = m} \frac{m!}{\alpha_1! \cdots \alpha_d!} \times \int_{\mathbb{R}^d} \left(\frac{\partial^m u}{\partial x_1^{\alpha_1} \cdots \partial x_d^{\alpha_d}} \right)^2 d\mathbf{x} \tag{3}$$

according to Duchon [6] and Wahba [20] with α_k being positive integers. The functional is invariant under similarity transformations. Note, that for the special case of $d = m = 2$ we obtain the functional originally used in [2].

Let a set of functions ϕ_ν span the space $\Pi^{m-1}(\mathbb{R}^d)$ of all polynomials on $\mathbb{R}^d$ up to order $m - 1$, which is the nullspace of the functional in (3). The dimension of this space is $M = (d + m - 1)!/(d!(m - 1)!)$ and must be lower than n. This condition determines the minimum number of landmarks, e.g., for $d = m = 2$ the number of landmarks must be larger than three. The solution of minimizing the functional in (3) can now be written in analytic form

$$u(\mathbf{x}) = \sum_{\nu=1}^{M} a_\nu \phi_\nu(\mathbf{x}) + \sum_{i=1}^{n} w_i U(\mathbf{x}, \mathbf{p}_i) \tag{4}$$

with basis functions $U(\mathbf{x}, \mathbf{p}_i)$ depending on 1) the dimension d of the domain; 2) the order m of the derivatives in the functional; and 3) the Hilbert space $\mathcal{H}$ of admissible functions. Choosing the space of functions on $\mathbb{R}^d$ for which all partial derivatives of total order m are square integrable, i.e., are in $L_2(\mathbb{R}^d)$, this results in the basis functions [see (5) at the bottom of the page.] with $\theta_{m,d}$ as defined in Wahba [20]. Note, that the basis functions $U(\mathbf{x}, \mathbf{p}_i)$ span an n-dimensional space of functions that depend only on the landmarks $\mathbf{p}_i$ of the first image. For $m = d = 2$ we have the well-known function $U(\mathbf{x}, \mathbf{p}) = 1/(8\pi)|\mathbf{x} - \mathbf{p}|^2 \ln|\mathbf{x} - \mathbf{p}|$ and the nullspace is spanned by $\phi_1(\mathbf{x}) = 1$, $\phi_2(\mathbf{x}) = x$, and $\phi_3(\mathbf{x}) = y$.

To compute the coefficients $\mathbf{a} = (a_1, \ldots, a_M)^T$ and $\mathbf{w} = (w_1, \ldots, w_n)^T$ of the analytic solution (4) we have to solve the following system of linear equations:

$$\begin{aligned} \mathbf{K}\mathbf{w} + \mathbf{P}\mathbf{a} &= \mathbf{v} \\ \mathbf{P}^T\mathbf{w} &= \mathbf{0} \end{aligned} \tag{6}$$

where $K_{ij} = U(\mathbf{p}_i, \mathbf{p}_j), P_{ij} = \phi_j(\mathbf{p}_i)$, and $\mathbf{v}$ is the column vector of one component of the coordinates of the landmarks $\mathbf{q}_i$ of the second image. The condition $\mathbf{P}^T\mathbf{w} = \mathbf{0}$ represents

$$U(\mathbf{x}, \mathbf{p}) = \begin{cases} \theta_{m,d}|\mathbf{x} - \mathbf{p}|^{2m-d} \ln|\mathbf{x} - \mathbf{p}|, & 2m - d \text{ even positive integer} \\ \theta_{m,d}|\mathbf{x} - \mathbf{p}|^{2m-d}, & \text{otherwise,} \end{cases} \tag{5}$$

the boundary conditions and ensures that the elastic part of the transformation is zero at infinity.

B. Extension from Interpolation to Approximation

With the interpolation approach described above the landmarks are matched exactly. This implicitly assumes that the landmark positions are known exactly. If we want to take into account landmark localization errors, we have to extend this approach by weakening the interpolation condition (1). This can be achieved by introducing a quadratic approximation term in the functional (2) which then reads as

$$J_\lambda(\mathbf{u}) = \frac{1}{n}\sum_{i=1}^{n}\frac{|\mathbf{q}_i - \mathbf{u}(\mathbf{p}_i)|^2}{\sigma_i^2} + \lambda J_m^d(\mathbf{u}). \tag{7}$$

Within the field of computer vision, functionals of this type have previously been considered for the reconstruction of surfaces from sparse depth data, i.e., for finding a mapping $u : \mathbb{R}^2 \rightarrow \mathbb{R}$ (e.g., [17]). Arad *et al.* [1] recently used a 2-D approximation approach of this kind to represent and modify facial expressions.

The first term of the functional in (7), the so-called data term, measures the sum of the quadratic Euclidean distances between the transformed landmarks $\mathbf{p}_i$ and the landmarks $\mathbf{q}_i$. Each distance can be weighted by the variances σ_i^2 representing landmark localization errors. If, for example, the variance is high, i.e., landmark localization is uncertain, then the influence on the overall approximation error is weighted low. Note, that we have only one parameter to represent the localization uncertainties of two corresponding landmarks. Thus, we have to combine the variances of corresponding landmarks. In our case, we use the sum of both variances, $\sigma_i^2 = \sigma_{i,\mathbf{p}}^2 + \sigma_{i,\mathbf{q}}^2$ (see also below).

The second term in (7) measures the smoothness of the resulting transformation. Hence, the minimization of the functional yields a transformation $\mathbf{u}$ which 1) approximates the distance between the landmark sets and 2) is sufficiently smooth. The relative weight between the approximation behavior and the smoothness of the transformation is determined by the regularization parameter $\lambda > 0$. If λ is small, we obtain a solution with good adaption to the local structure of the deformations and if λ is large, we obtain a very smooth transformation with little adaption to the deformations. There are two limiting cases: For $\lambda \rightarrow 0$ we obtain the original interpolating thin-plate spline transformation, and for $\lambda \rightarrow \infty$ we have a global polynomial of order up to $m-1$, which has no bending energy at all. Choosing $m = 2$ in the latter case results in an affine transformation. Thus, for $m = 2$ and general values of $\lambda > 0$, we obtain an approximating elastic transformation the behavior of which lies in the range between the two extremes of the interpolating thin-plate spline transformation and an approximating affine transformation.

The interesting fact is that the solution to the approximation problem (7) can also be stated analytically and consists of the same basis functions as in the case of interpolation (Duchon [6] and Wahba [20]). The computational scheme to compute the coefficients of the transformation $\mathbf{u}$ is nearly the same

$$\begin{aligned}(\mathbf{K} + n\lambda\mathbf{W}^{-1})\mathbf{w} + \mathbf{P}\mathbf{a} &= \mathbf{v}\\ \mathbf{P}^T\mathbf{w} &= \mathbf{0}\end{aligned} \tag{8}$$

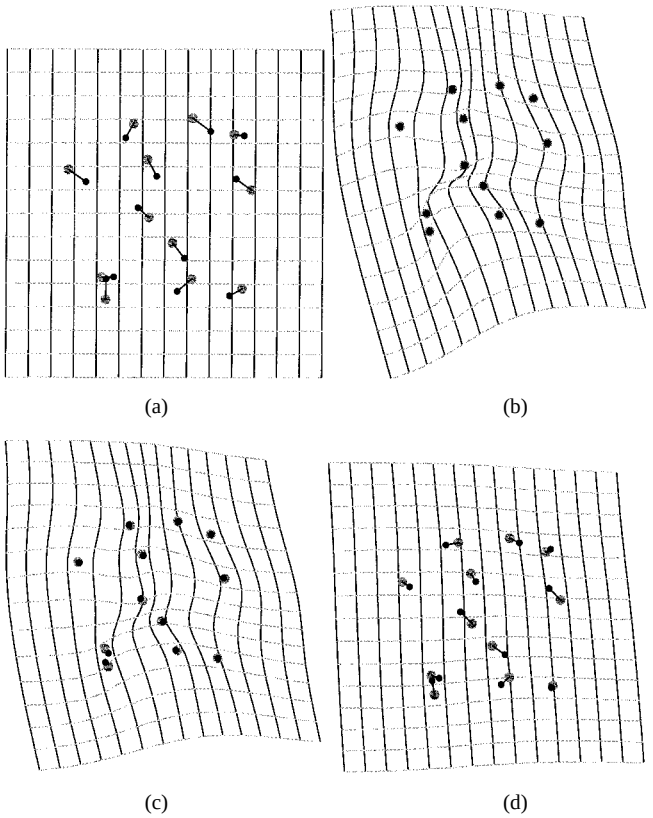

Fig. 1. (a)–(d) Performance of approximating thin-plate splines visualized by deforming a regular grid: Two different landmark sets represented by the small black dots and the larger grey dots, interpolation ($\lambda = 0$), approximation (intermediate value of $\lambda = 0.001$), and nearly affine approximation (large value of $\lambda = 0.1$).

where

$$\mathbf{W}^{-1} = \begin{pmatrix}\sigma_1^2 & & \mathbf{0}\\ & \ddots & \\ \mathbf{0} & & \sigma_n^2\end{pmatrix} \tag{9}$$

In comparison to the interpolating case, we only have to add $n\lambda\mathbf{W}^{-1}$ in the diagonal of the matrix $\mathbf{K}$. As a by-product, this results in a better conditioned linear system of equations yielding a more robust numerical solution. To refer to these splines resulting from the stated approximation problem we here use the term *approximating thin-plate splines*. Note, that in the mathematical literature generally the term *thin-plate smoothing spline* is used (e.g., [20]).

The transformation behavior of the thin-plate spline approximation scheme can be visualized by deforming a regular grid. Fig. 1 shows an example for different values of λ while setting $m = 2$ and assuming equal weights $\sigma_i = 1$. In Fig. 1(a) are shown the landmarks of the first and second image marked on a regular grid by the small black dots and the larger grey dots, respectively. Fig. 1(b) shows the transformation result for $\lambda = 0$, which is the case of thin-plate spline interpolation, where the landmarks are matched exactly. For an intermediate value of $\lambda = 0.001$, we obtain an approximation behavior with generally smaller local deformations [Fig. 1(c)]. A much larger value of $\lambda = 0.1$ yields a nearly pure affine transformation with hardly any local deformations [Fig. 1(d)].

C. Incorporation of Anisotropic Landmark Errors

The approximation scheme described above uses scalar weights to represent landmark localization errors. This, however, implies isotropic localization errors and is only a coarse error characterization. Generally, the errors are different in different directions and thus are anisotropic. A further extension of the approach from above is obtained by replacing the scalar weights σ_i^2 with weight matrices Σ_i representing anisotropic landmark localization errors. For 3-D images, for example, the weight matrices are 3×3 covariance matrices. Now the functional reads as

$$J_\lambda(\mathbf{u}) = \frac{1}{n}\sum_{i=1}^{n}(\mathbf{q}_i - \mathbf{u}(\mathbf{p}_i))^T\Sigma_i^{-1}(\mathbf{q}_i - \mathbf{u}(\mathbf{p}_i)) + \lambda J_m^d(\mathbf{u}). \tag{10}$$

Indeed, also for this generalized functional the solution can be stated in analytic form with the same basis functions as before (see Wahba [20] and Wang [21] for a theoretical treatment of such functionals). The computational scheme to compute the coefficients of the transformation $\mathbf{u}$ has the same structure as (8), however, a separation into the components u_k of the transformation $\mathbf{u}$ is no longer possible. Now, the weighting matrix in (8) represents the covariance matrices $\Sigma_i, i = 1 \ldots n$, of the landmarks through

$$\mathbf{W}^{-1} = \begin{pmatrix} \Sigma_1 & & \mathbf{0} \\ & \ddots & \\ \mathbf{0} & & \Sigma_n \end{pmatrix} \tag{11}$$

which is a block-diagonal matrix. Note, that the mathematical work in, e.g., [21], treats the more general case of $\mathbf{W}^{-1}$ being a dense matrix. In medical image registration, however, a block-diagonal matrix is sufficient. While the errors for a single landmark are generally correlated, it can well be assumed that there is no correlation between *different* landmarks.

Note also, that the Σ_i represent the localization errors of two corresponding landmarks. Thus, to end up with one matrix we have to combine the covariance matrices of corresponding landmarks. If we assume that the corresponding two covariance matrices depend only slightly on the elastic part of the transformation, then we can combine these matrices by applying a linear transformation which allows for rotation and scaling, i.e., $\Sigma_i = \mathbf{A}\Sigma_{i,\mathbf{p}}\mathbf{A}^T + \Sigma_{i,\mathbf{q}}$, where the matrix $\mathbf{A}$ can be computed based on all landmarks. If we can further assume that the images have approximately the same orientation and scale then we can simply add the two covariance matrices. The other matrices in the linear system of (8) are given by $\mathbf{K} = (K_{ij}\mathbf{I}_d)$, where $K_{ij} = U(\mathbf{p}_i, \mathbf{p}_j)$ and $\mathbf{I}_d$ is the $d \times d$ identity matrix, and $\mathbf{P} = (P_{ij}\mathbf{I}_d)$, where $P_{ij} = \phi_j(\mathbf{p}_i)$.

With the extended approximation scheme it is possible to include different types of 3-D point landmarks, e.g., "normal" point landmarks as well as "quasi-landmarks." Normal point landmarks have a unique position and low localization uncertainties in all directions. An example for quasi-landmarks are arbitrary edge points. Such points are not uniquely definable in all directions, and they are used, for example, in the reference system of Talairach [16] to define the 3-D bounding box of the human brain. The incorporation of such landmarks is important since normal point landmarks are hard to define, for example, at the outer parts of the human head.

Note, that the above introduced approximation scheme using weight matrices is also a generalization of the work in Bookstein [4], where the interpolation problem is solved while the landmarks are allowed to slip along straight lines within a 2-D image. Actually, this is a special case of our approximation scheme since for straight lines the variance in one direction is zero whereas in the perpendicular direction it is infinite.

III. Semi-Automatic Localization of Anatomical Landmarks

Anatomical point landmarks in 3-D tomographic datasets are usually localized manually. Generally, this procedure is difficult, time-consuming, and often lacks accuracy. To improve on this, we use a semi-automatic scheme in conjunction with 3-D differential operators. In comparison to an automatic procedure, such a semi-automatic approach has the advantage that the user has the possibility to control the results ("keep-the-user-in-the-loop" paradigm).

As 3-D differential operators we apply 3-D extensions of 2-D corner operators (Rohr [12]). Recently, we have evaluated a larger number of 3-D differential operators using different performance criteria (Hartkens *et al.* [9]). The investigated operators are based on either first or first- and second-order partial derivatives of an image. Examples of the latter type of operators are based on the mean and Gaussian curvature of isocontours. These operators are related to approaches which utilize curvature properties of isocontours for detecting 3-D crest or ridge lines. In comparison to the 3-D operators in [12] and [9] the crest-line based approach of Thirion [18] requires third-order image derivatives to determine extremal points. In our evaluation study in [9] it turned out that the operators based on only first-order image derivatives yield the best results. Therefore, we use them in our application.

A. Semi-Automatic Scheme for Landmark Localization

To localize a certain 3-D anatomical point landmark we apply the following user-interaction scenario: 1) the user specifies a region of interest (ROI) together with an approximate position (e.g., the center of the ROI); 2) a 3-D differential operator is applied yielding landmark candidates within the selected ROI; and then 3) the user selects the most promising candidate. To simplify the selection procedure, the landmark candidates may be ordered either based on their operator responses or on their distances to the manually specified position.

The anatomical landmarks we use are landmarks on the skull (e.g., tip of external protuberance, saddle point on the zygomatic bone, and saddle point on the mastoid process) as well as landmarks on the ventricular system (e.g., tips of frontal, occipital, and temporal horns, topmost concavity of fourth ventricle roof, and tip between medulla oblongata and pons). These landmarks are visible both in MR as well as CT images and can be geometrically characterized as tips or saddle points.

B. Three-Dimensional Extensions of Corner Detectors

For landmark detection we apply 3-D differential operators which are extensions of existing 2-D corner detectors used to detect points of high intensity variations. These operators are based on only first-order partial derivatives of an image. Therefore, these operators are computationally efficient and do not suffer from instabilities of computing high order partial derivatives. Let the matrix $\mathbf{C}_g = \overline{\nabla g (\nabla g)^T}$ denote the averaged dyadic product of the 3-D grey-value gradient $\nabla g = (g_x, g_y, g_z)^T$, then we can define the following three operators [12]:

$$\frac{\det \mathbf{C}_g}{\mathrm{trace}\mathbf{C}_g}, \quad 1/\mathrm{trace}\mathbf{C}_g^{-1}, \quad \det \mathbf{C}_g. \tag{12}$$

Local maxima of these operators serve as landmark candidates within the above described semi-automatic scheme (for details, see [12]).

IV. Experimental Results

We now present experimental results of applying the approximating thin-plate spline registration scheme to 2-D as well as 3-D image data. In the experiments we treat the cases of equal isotropic landmark errors, individual isotropic errors, as well as individual anisotropic errors.

A. Two-Dimensional Data

Within the task of MR-CT registration we here consider the application of correcting patient-induced susceptibility distortions of MR images. We have acquired two sagittal MR brain images of size 256 $\times$ 256 pixels with typical susceptibility distortions of a healthy human volunteer. In our experiment we used a high-gradient MR image as "ground truth" (instead of clinically common CT images) to avoid exposure of the volunteer to radiation. Both turbo-spin echo images have consecutively been acquired on a modified Philips 1.5-T MR scanner with a slice thickness of 4 mm without repositioning. Therefore, we are sure that we actually have identical slicing in space. Using a gradient of 1 mT/m and 6 mT/m for the first and second image, then leads to a shift of ca. $7.5 \ldots 10$ mm and ca. $1.3 \ldots 1.7$ mm, respectively.

Within each of the two images we have manually specified 20 point landmarks [see Fig. 2(a), (b)]. To simulate large landmark localization errors, one of the landmarks in the second image (no. 3) has been shifted about 15 pixels away from its true position. This large shift has been chosen for demonstration purposes. Note, however, that manual localization can actually be prone to relatively large errors. Fig.2 shows the results of interpolating thin-plate splines [Fig.2(c)] versus approximating thin-plate splines setting $m = d = 2$ and using equal scalar weights $\sigma_i = 1$ [Fig.2(d)]. For the regularization parameter, we have used a value of $\lambda = 50$. Note, that for a comparison of this value with the values used in the synthetic experiment in Fig. 1, one has to keep in mind that there a (normalized) image dimension of 1×1 pixels has been used. Thus, we have to normalize the regularization parameter to the current image dimension. Doing this, we obtain $\lambda_{\mathrm{norm}} = 50/(256^2) \approx 0.0008$, which corresponds to the intermediate value of λ in Fig. 1. Each result in Fig. 2(c), (d) represents the transformed first image. It can be seen that the interpolation scheme yields a rather unrealistic deformation since it forces all landmark pairs, including the pair with the simulated localization error, to exactly match each other. Using the approximation scheme instead yields a more accurate registration result. In the difference image of the two results in Fig. 2(e) we see that the largest differences occur at the shifted landmark no. 3 which is what we expect. The increased accuracy of the approximation scheme can also be demonstrated by computing the distance between the grey-value edges of the transformed images and those of the second image. In our case, we applied a distance transformation to computed grey-value edges. The results for the marked rectangular image parts in Fig. 2(c), (d) can be seen in Fig. 2(f), (g). Here, the grey values represent the registration error, i.e., the brighter the larger is the error. In particular at the marked circular areas, which indicate the grey-value edges perpendicular to the simulated shift, we see that the registration accuracy has increased significantly.

B. Three-Dimensional Data

Next, we show experimental results of applying the approximating thin-plate spline approach to 3-D atlas data. In our experiment we have simulated nonlinear deformations of the digital SAMMIE atlas (Hübner *et al.* [10]). This 3-D human brain atlas consists of 110 slices each of 270 $\times$ 346 pixels resolution. One slice is shown in Fig. 3(a). Different anatomical structures are labeled with different gray values. The deformed atlas with overlaid contours from the original atlas is shown on the right. It can be seen that the deformations are relatively large [see also the enlarged sections in Fig. 4 (a), (b)]. For the deformation we used a nonlinear function that depends on the angle between the top-left and the bottom-right diagonal of the image, with the largest deformation in the direction of the bottom-left diagonal of the image. Note, that the simulated nonlinear deformation does not lie within the function space of thin-plate splines or polynomials. To register the deformed atlas with the original atlas, we have manually specified 34 homologous landmarks and have added Gaussian noise to the landmark positions such as to simulate typical localization errors. A different noise level has been chosen for each landmark, with standard deviations $\sigma_{n,i}$ in the range between 0.5 and 3.5 voxels. For our experiment this resulted in displacements between 0.5 and 7 voxels which are to be expected for manual landmark localization. Fig. 4(d) shows the result of the approximating thin-plate spline approach ($m = 2$ and $d = 3$) in comparison to an optimal affine transformation (limiting case $\lambda = \infty$ of approximating thin-plate splines) [Fig. 4(c)]. For the scalar weights we have used values in accordance with the simulated noise levels. Note, that with both transformation functions we have used the same input information consisting of the positions of the landmarks as well as their localization uncertainties (this is analogous to the experiment above). However, as can be seen, the registration result with approximating thin-plate splines is significantly better in comparison to an optimal affine transformation, particularly in the lower part of the image.

We have also applied our approach to the registration of 3-D MR and CT images. The MR dataset consists of 120 axial slices of 256 $\times$ 256 resolution with an intensity range of 0–299, while the CT dataset consists of 87 axial slices of 320 $\times$ 320 res-

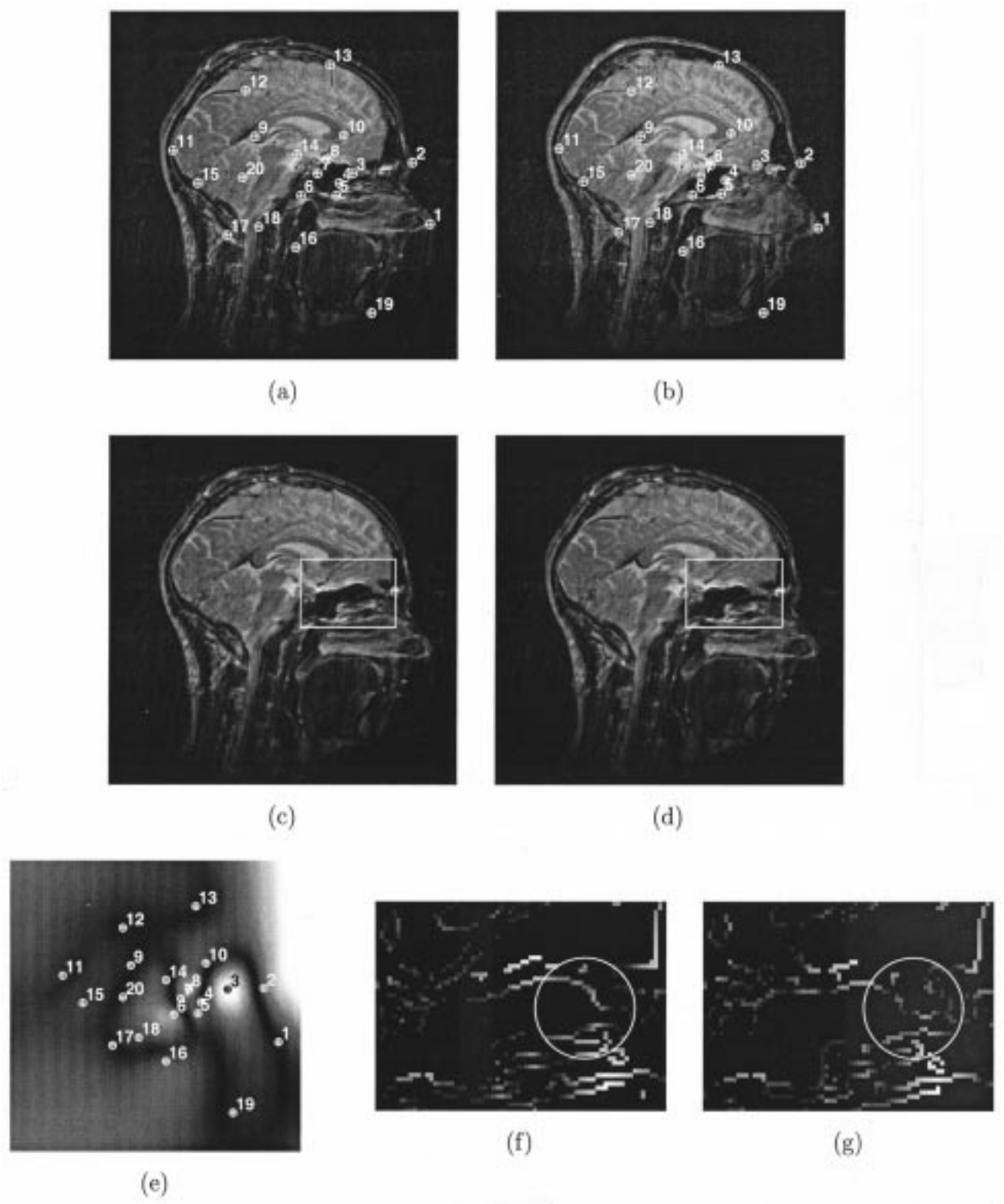

Fig. 2. Two-dimensional MR images of the same patient with marked landmarks. First, (a) low-gradient image and second (b) high-gradient image. Two-dimensional registration result (transformed first image): (c) Interpolating thin-plate splines and (d) approximating thin-plate splines using equal scalar weights. (e) Difference between the two registration results. Registration errors for the marked image parts in (c) and (d) using (f) interpolating thin-plate splines and (g) approximating thin-plate splines using equal scalar weights.

olution with an intensity range of 0–3207. The images have been acquired from the same patient [see Fig. 5 (a), (b) for slices 34 and 38 of the original images, respectively]. In this example, the landmarks have been localized semi-automatically using the 3-D differential operator $\det\mathbf{C}_g$ in (12). For registration we have applied the approximating thin-plate spline approach with incorporated weight matrices as given in (10) using $m = 2$ and $d = 3$. The weight matrices have been specified in

(a) (b)

Fig. 3. (a) Original and (b) analytically deformed 3-D human brain atlas (slice 45 of the SAMMIE atlas).

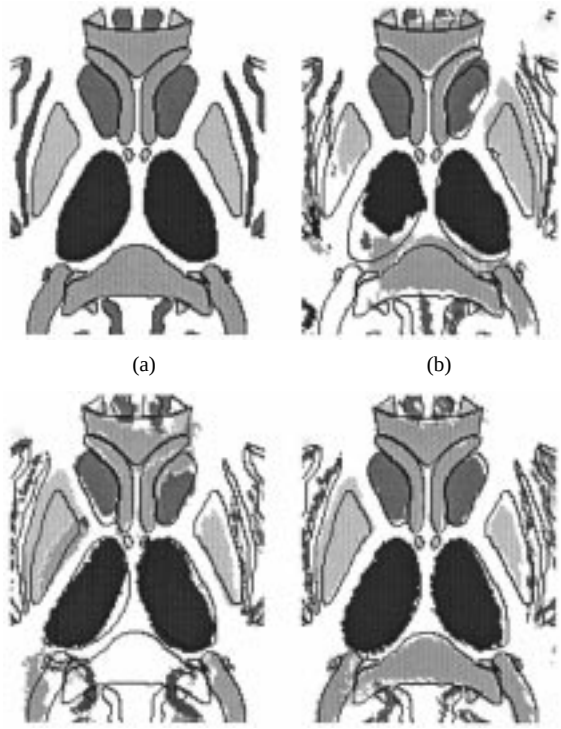

(a) (b)

(c) (d)

Fig. 4. (a) Section of the 3-D human brain atlas and (b) 3-D registration result using individual scalar weights. (c) Optimal affine approximation. (d) Thin-plate spline approximation.

the following way (Rohr [13]). In a local 3-D window around the detected landmark we analyze the local grey-value variations and estimate the minimal localization uncertainty for this point which is given by the Cramér–Rao bound (van Trees [19]): $\Sigma_g = (\sigma_n^2/m)\mathbf{C}_g^{-1}$, where σ_n^2 denotes the variance of additive white Gaussian image noise, m the number of voxels in the local 3-D window, and $\mathbf{C}_g = \overline{\nabla g(\nabla g)^T}$ is the averaged dyadic product of the image gradient. In our case, we used a window size of $5 \times 5 \times 5$ voxels. From the estimated covariance matrices we can compute the 3-D error ellipsoids with principal axes σ_x, σ_y, and σ_z. Our results show that the estimated error ellipsoids are well adapted to the local structure of the image. For a landmark with high intensity variations the localization uncertainty is low and vice versa. Note, that the incorporated covariance matrices represent lower bounds for the localization uncertainties. An alternative approach would be to exploit anatomical knowledge about the localization uncertainties of landmarks. In general, these uncertainties are different and higher (or at most equal) in comparison to the lower bounds. However, since currently we have no such knowledge about the landmarks we prefer to use the lower bounds. An advantage of our approach is that we can incorporate different types of landmarks, i.e., besides unique point landmarks we can also incorporate quasi-landmarks, e.g., arbitrary edge points in 3-D. For such points the localization uncertainties in different directions differ largely. Below, we report on an example of incorporating such types of landmarks. For the current example of 3-D MR-CT registration we have used only unique point landmarks. For all landmarks the corresponding covariance matrices have been estimated automatically from the image data as described above. Fig. 5(c) shows the registration result for slice 38 by superimposing 3-D Canny edges of the CT image on the transformed MR image. It can be seen that the registration accuracy is rather good. We here have used a value of $\lambda = 3000$ which corresponds to a normalized value of $\lambda_{\text{norm}} \approx 0.0004$ (using the average dimension of both images). However, for these datasets it turns out that the registration accuracy is nearly independent of the parameter λ. Thus, in the case when the distortions of the MR image can be assumed to be small, an optimal affine transformation seems to be sufficient.

In the last example, we demonstrate the application of the approximating thin-plate spline approach to the registration of 3-D MR images of different patients. The datasets consist of $179 \times 236 \times 165$ and $177 \times 245 \times 114$ voxels, respectively Also, with this example, we have used $m = 2$ and $d = 3$, and the point landmarks have been localized semi-automatically using the 3-D differential operator $\det\mathbf{C}_g$ in (12). The used point landmarks are the topmost concavity of the fourth ventricle, the tips of the frontal ventricular horns (l, r), the tips of the temporal ventricular horns (l, r), the saddle points at the zygomatic bones (l, r), the genu of corpus callosum, the upper junction at the pons, and the lower junction at the pons. Three of these landmarks can be found in both hemispheres which has been indicated by (l, r). Additionally, we here have incorporated quasi-landmarks, namely the 3-D bounding box landmarks of the brain as used in the reference system of Talairach [16] as well as two landmarks at the top of the ventricular system. The six bounding box landmarks in [16] are the uppermost point of the parietal cortex, the lowest point of the temporal cortex, the most anterior point of the frontal cortex, the most posterior point of the occipital cortex, the most lateral point of the left parieto-temporal cortex, and the most lateral point of the right parieto-temporal cortex. The quasi-landmarks have been localized manually. In summary, we have used ten normal point landmarks and eight quasi-landmarks. For all landmarks (normal and quasi-landmarks) the covariance matrices have been estimated automatically from the image data as described above. As above in the MR-CT example we have used for the regularization parameter a value of $\lambda = 3000$, which here corresponds to a normalized value of $\lambda_{\text{norm}} \approx 0.0005$ (using the average dimension of both images). Fig. 6(b) shows that we generally obtain a

(a) (b) (c)

Fig. 5. Three-dimensional (a) MR and (b) CT datasets of the same patient (slices 34 and 38, respectively). (c) Three-dimensional registration result using approximating thin-plate splines and estimated 3-D covariance matrices (slice 38).

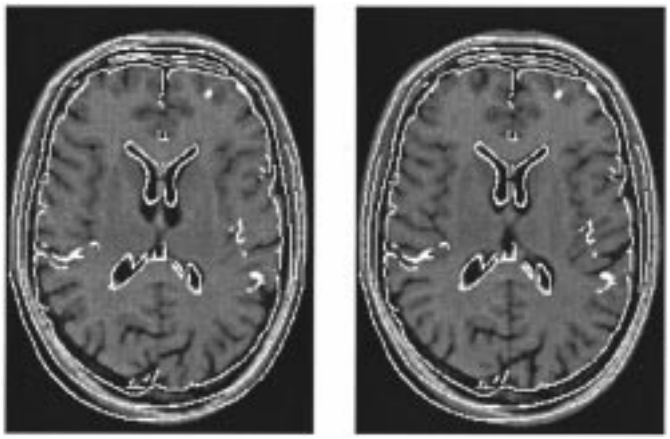

(a) (b)

Fig. 6. Three-dimensional registration result (a) using interpolating thin-plate splines, normal landmarks, and quasi-landmarks and (b) using approximating thin-plate splines, normal landmarks, quasi-landmarks, and estimated 3-D covariance matrices (slice 67).

good registration result while some deviations can be observed at the bottom-left. The registration accuracy is improved in comparison to using interpolating thin-plate splines in Fig. 6(a). This can be seen, for example, at the ventricular system.

ACKNOWLEDGMENT

The authors would like to thank K. Jungnickel for providing the MR images showing the susceptibility distortions. They would also like to thank W. P. Th. M. Mali, L. Ramos, and C. W. M. van Veelen (Utrecht University Hospital) for providing the 3-D MR and CT images via ICS-AD of Philips Medical Systems Best. Finally, they would like to thank F. J. Schuier and T. Wittkopp for making available the SAMMIE atlas developed within the EU project SAMMIE (Contract A2032).

REFERENCES

[1] N. Arad, N. Dyn, D. Reisfeld, and Y. Yeshurun, "Image warping by radial basis functions: Application to facial expressions," *Comput. Vis., Graph., Image Processing*, vol. 56, no. 2, pp. 161–172, 1994.

[2] F. L. Bookstein, "Principal warps: Thin-plate splines and the decomposition of deformations," *IEEE Trans. Pattern Anal. Machine. Intell.*, vol. 11, pp. 567–585, June 1989.

[3] ——, "Four metrics for image variation," in *Proc. 11th Int. Conf. Information Processing in Medical Imaging (IPMI'89), Progress in Clinical and Biological Research*, vol. 363, D. Ortendahl and J. Llacer, Eds., 1991, pp. 227–240.

[4] ——, "Landmark methods for forms without landmarks: Morphometrics of group differences in outline shape," *Med. Image Anal.*, vol. 1, no. 3, pp. 225–243, 1996/1997.

[5] G. E. Christensen, S. C. Joshi, and M. I. Miller, "Volumetric transformation of brain anatomy," *IEEE Trans. Med. Imag.*, vol. 16, no. 6, pp. 864–877, Dec. 1997.

[6] J. Duchon, "Interpolation des fonctions de deux variables suivant le principe de la flexion des plaques minces," *R.A.I.R.O. Analyze Numérique*, vol. 10, no. 12, pp. 5–12, 1976.

[7] A. C. Evans, W. Dai, L. Collins, P. Neelin, and S. Marrett, "Warping of a computerized 3-D atlas to match brain image volumes for quantitative neuroanatomical and functional analysis," in *Proc. SPIE 1445 Medical Imaging V: Image Processing*, M. H. Loew, Ed., San Jose, CA, 1991, pp. 236–246.

[8] J. C. Gee, D. R. Haynor, M. Reivich, and R. Bajcsy, "Finite element approach to warping of brain images," in *Proc. SPIE 2167 Medical Imaging 1994: Image Processing*, M. H. Loew, Ed., Newport Beach, CA, USA, Feb. 15–18, 1994, pp. 327–337.

[9] T. Hartkens, K. Rohr, and H. S. Stiehl, "Performance of 3D differential operators for the detection of anatomical point landmarks in MR and CT images," in *Proc. SIE Int. Symp. Medical Imaging 1999—Image Processing (MI'99)*, vol. 3661, K. M. Hanson, Ed., San Diego, CA, Feb. 22–25, 1999, pp. 32–43.

[10] U. Hübner, F. J. Schuier, and J. A. Newell, "Software applied to multimodal images and education," *Comput. Meth. Programs Biomed.*, vol. 45, pp. 149–152, 1994.

[11] K. Mardia, J. T. Kent, C. R. Goodall, and J. Little, "Kriging and splines with derivative information," *Biometrika*, vol. 83, no. 1, pp. 207–221, 1996.

[12] K. Rohr, "On 3D differential operators for detecting point landmarks," *Image Vis. Computing*, vol. 15, no. 3, pp. 219–233, 1997.

[13] ——, "Image registration based on thin-plate splines and local estimates of anisotropic landmark localization uncertainties," in *Proceedings First International Conference on Medical Image Computing and Computer-Assisted Intervention (MICCAI'98)*. ser. Lecture Notes in Computer Science, W. M. Wells, A. Colchester, and S. Delp, Eds. Berlin, Germany: Springer Verlag, Oct. 11–13, 1998, vol. 1496, pp. 1174–1183.

[14] K. Rohr, H. S. Stiehl, R. Sprengel, W. Beil, T. M. Buzug, J. Weese, and M. H. Kuhn, "Point-based elastic registration of medical image data using approximating thin-plate splines," in *Proceedings Fourth International Conference on Visualization in Biomedical Computing (VBC'96)*. ser. Lecture Notes in Computer Science, K. H. Höhne and R. Kikinis, Eds. Berlin, Germany: Springer, Sept. 22–25, 1996, vol. 1131, pp. 297–306.

[15] K. Rohr, R. Sprengel, and H. S. Stiehl, "Incorporation of landmark error ellipsoids for image registration based on approximating thin-plate splines," in *Proc. Computer Assisted Radiology and Surgery (CAR'97)*, H. U. Lemke, M. W. Vannier, and K. Inamura, Eds., June 25–28, 1997, pp. 234–239.

[16] J. Talairach and P. Tornoux, *Co-Planar Stereotactic Atlas of the Human Brain*. Stuttgart, Germany: Georg Thieme Verlag, 1988.

[17] D. Terzopoulos, "Regularization of inverse visual problems involving discontinuities," *IEEE Trans. Pattern Anal. Machine Intell.*, vol. PAMI-8, no. 4, pp. 413–424, 1986.

[18] J.-P. Thirion, "New feature points based on geometric invariants for 3-D image registration," *Int. J. Comput. Vis.*, vol. 18, no. 2, pp. 121–137, 1996.

[19] H. L. van Trees, *Detection, Estimation, and Modulation Theory*. New York: Wiley, 1968, pt. I.

[20] G. Wahba, *Spline Models for Observational Data*. Philadelphia, PA: Soc. Ind. Appl. Math., 1990.

[21] Y. Wang, "Smoothing spline models with correlated random errors," *J. Amer. Statist. Assoc.*, vol. 93, no. 441, pp. 341–348, 1998.